Transfer functions in lensless ghost-imaging systems

Jing Cheng
Department of Physics, South China University of Technology, Guangzhou 510640, China
(Received 4 May 2008; revised manuscript received 6 August 2008; published 27 October 2008)

Transfer functions are of fundamental importance in analyzing the image formation in optical imaging systems. For the recently proposed lensless ghost-imaging systems, when a pointlike or bucket detector is used in the measurement, the corresponding amplitude transfer functions or optical transfer functions are derived. Defocusing effects are also investigated. With the help of these transfer functions, we can quantitatively study the imaging ability of lensless ghost-imaging systems.

DOI: 10.1103/PhysRevA.78.043823 PACS number(s): 42.30.Lr, 42.30.Va, 42.25.Kb, 42.50.Ar

I. INTRODUCTION

Recently, a new kind of imaging technique, ghost imaging (GI), has attracted much interest from investigators and practitioners in the field of quantum optics [1]. GI is a kind of nonlocal imaging method. By correlating the intensity fluctuations of two spatially correlated beams that travel through two different imaging systems, an unknown object in the test imaging system can be nonlocally retrieved on the detector of the other reference imaging system. Both quantum entangled and classically correlated incoherent light sources can be used to realize GI [2–9]. A very interesting advantage of the use of incoherent sources is that they can be used to generate images without the use of lenses. Lensless imaging is very useful in many applications. Cheng and Han first discussed the possibility of realizing lensless Fourier transform imaging and its applicability in x-ray diffraction [4,10]. Soon after, it was shown that true images also can be produced from a lensless ghost-imaging (LGI) system [11,12].

In optical imaging theory, the concept of the transfer function is of fundamental importance and has been widely used to describe image formation in an optical imaging system [13]. Depending on whether the imaging system is coherent or incoherent, either the amplitude transfer function (ATF, also known as the coherent transfer function) or the optical transfer function (OTF) can be used to analyze the imaging process. It is well known that a ghost-imaging system can be used to realize both coherent and incoherent imaging functions when a pointlike or bucket detector is used. To our knowledge, there have been no studies on the ATF and OTF in LGI systems. The purpose of this paper is to derive the ATF and OTF in LGI systems, and use them to discuss the imaging quality.

The paper is organized as follows. In Sec. II, we study the ATF in a LGI system with a pointlike test detector. When a bucket detector is used, the LGI system is effectively an incoherent imaging system; the corresponding OTF is derived in Sec. III. In Sec. IV, we discuss defocusing effects; the defocused ATF and OTF are given. Numerical simulations are given in Sec. V. Finally, conclusions are presented in Sec. VI.

II. AMPLITUDE TRANSFER FUNCTION IN A LGI SYSTEM WITH A POINTLIKE DETECTOR

A schematic diagram of a LGI system is shown in Fig. 1. An incoherent source is split into two beams by the beam splitter (BS). One is transmitted through a test path in which an object is located, and the other is transmitted through a reference path which is a path of free space. Two detectors D_t and D_r record the intensity distribution. A correlator is used to measure the correlation function of the intensity fluctuations. Here, $t(v)$ denotes the amplitude transmittance of the object, with v the transverse coordinate at the object plane. For simplicity, we only explicitly write a single transverse variable, but inclusion of the other variable is straightforward.

Based on classical optical coherence theory [14], the ghost image is proportional to the correlation between the intensity fluctuations [1]:

$$g_2(u,u') = \langle I_t(u')I_r(u)\rangle - \langle I_t(u')\rangle\langle I_r(u)\rangle = |\Gamma(u,u')|^2, \quad (1)$$

where Γ is the second-order cross-correlation function between the fields in the two detectors. From the propagation of the second-order correlation function [14],

$$\Gamma(u,u') = \int dx\, dv\, I_s(x)\exp\left(-\frac{i\pi}{\lambda z_1}(x-v)^2\right)t(v) \times\exp\left(-\frac{i\pi}{\lambda z_0}(v-u')^2\right)\exp\left(\frac{i\pi}{\lambda z_2}(x-u)^2\right), \quad (2)$$

where $I_s(x)$ is the intensity distribution of the source. Substituting Eq. (2) into Eq. (1), we have

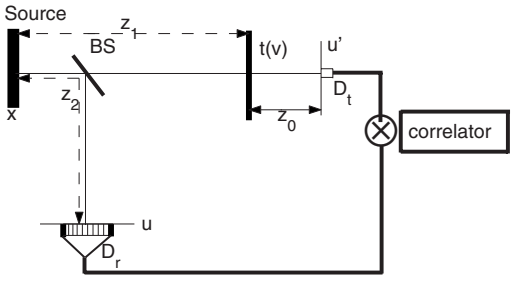

FIG. 1. Geometry of a LGI system. An incoherent source is split into two beams by the beam splitter (BS). z_1, z_2, and z_0 are the distances from the source to the unknown object, from the source to the reference detector D_r, and from the object to the test detector D_t, respectively. x, v, u, and u' are the coordinates at the source plane, object plane, reference detector plane, and test detector plane.

$$g_2(u,u') = \left| \int dv\ t(v) \exp\left(-\frac{i\pi}{\lambda z_0}(v-u')^2 - \frac{i\pi v^2}{\lambda z_1} + \frac{i\pi u^2}{\lambda z_2} \right) \times \int dx\ I_s(x) e^{-(i\pi/\lambda)(1/z_1 - 1/z_2)x^2} e^{(i2\pi/\lambda)(v/z_1 - u/z_2)x} \right|^2. \tag{3}$$

Neglecting the unrelated phase factors, and introducing a kernel function $h(u,v)$, we have

$$g_2(u,u') = \left| \int dv\ t(v) e^{-(i\pi/\lambda)(1/z_0 + 1/z_1)v^2} e^{(i2\pi/\lambda z_0)u'v} h(u,v) \right|^2, \tag{4}$$

where

$$h(u,v) = \int dx\ I_s(x) e^{-(i\pi/\lambda)(1/z_1 - 1/z_2)x^2} e^{(i2\pi/\lambda)(v/z_1 - u/z_2)x}. \tag{5}$$

Equations (4) and (5) comprise the starting point of our analysis in this paper. When the imaging condition $z_1 = z_2$ is satisfied, and a pointlike detector D_t located at $u' = 0$ is used, the ghost image will be

$$I(u) = g_2(u' = 0, u) = \left| \int dv\ t(v) e^{-(i\pi/\lambda)(1/z_0 + 1/z_1)v^2} \tilde{I}_s\left(\frac{u-v}{\lambda z_1} \right) \right|^2, \tag{6}$$

where $\tilde{I}_s(k)$ is the Fourier transform of $I_s(x)$. As in the imaging theory of a lens [13], the quadratic phase term in Eq. (6) can be removed if $\tilde{I}_s(k)$ falls off quickly as long as k is not equal to zero. Then the imaging formula in a LGI system with a pointlike D_t is

$$I(u) = \left| t(u) \otimes \tilde{I}_s\left(\frac{u}{\lambda z_1} \right) \right|^2, \tag{7}$$

where $\otimes$ denotes the convolution operation. This equation has the same formula as in a coherent lens imaging system; thus we obtain the ATF of a LGI system with a pointlike D_t, which is the Fourier transform of $\tilde{I}_s(u/\lambda z_1)$:

$$H_c(f) = I_s(-\lambda z_1 f), \tag{8}$$

where f is the spatial frequency related to the coordinates in the real spaces. With the help of the ATF and the convolution theorem, denoting $T(f)$ as the Fourier transform of $t(v)$, Eq. (7) can be represented as

$$I(u) = \left| \int T(f) H_c(f) e^{i2\pi u f} df \right|^2, \tag{9}$$

which clearly describes the image formation as a kind of filtering process in the frequency domain. To generate high-quality images, the ATF $H_c(f)$ should have a large bandwidth to allow the frequency components of the object to have small distortions.

For example, if $I_s(\vec{x})$ is uniformly distributed and has a circle shape with a radius of a_0, the corresponding ATF is the same as in a coherent thin lens imaging system [13]. So we can effectively realize coherent imaging by using an incoherent source and without using lenses. This result obviously may be very useful in cases where neither coherent sources nor optical lenses are accessible, as in x-ray optics. Increasing a_0 will increase the bandwidth, leading to improvement of the imaging quality.

Since in experiments $I_s(x)$ always has some distribution, let us consider a more realistic example. Suppose the incoherent source is a Gaussian function, i.e., $I_s(x) = \exp(-x^2/a_0^2)$, in which all transverse coordinates are included, then $\tilde{I}_s(u) = e^{-\pi^2 a_0^2 u^2}$, and we find that the ATF is

$$H_c(f) = \exp\left(-\frac{\lambda^2 z_1^2 f^2}{a_0^2} \right).$$

$H_c(f)$ falls quickly at large f. So we can determine a cutoff frequency $f_c = (3/\sqrt{2})a_0/(\lambda z_1)$, which is defined as three times the standard deviation of $|H_c(f)|$. Increasing the size of the source can increase the cutoff frequency. From the transfer function analysis, detailed structures of the object corresponding to frequencies larger than f_c cannot be imaged through the LGI system.

III. OPTICAL TRANSFER FUNCTION IN A LGI SYSTEM WITH A BUCKET DETECTOR

In the previous section, our analysis was based on the use of a pointlike detector D_t. Actually, there are some experiments in which D_t is pointlike, as in Ref. [10]. However, in many other experiments, D_t is a bucket detector. So another kind of transfer function is needed to study these schemes.

We introduce a detector function $d(x)$ to describe the bucket detector; $d(x) = 1$ if x is inside D_t while $d(x) = 0$ if x is outside D_t. Then the measured ghost image will be proportional to

$$I(u) = \int du' d(u') g_2(u,u'). \tag{10}$$

Substituting Eqs. (4) and (5) and suppose the imaging condition is satisfied ($z_1 = z_2$), we have

$$\begin{aligned} I(u) &= \int du' d(u') \int dv_1 t(v_1) e^{(i2\pi/\lambda z_0)u'v_1} \tilde{I}_s\left(\frac{u-v_1}{\lambda z_1} \right) \times \int dv_2 t^*(v_2) e^{-(i2\pi/\lambda z_0)u'v_2} \tilde{I}_s^*\left(\frac{u-v_2}{\lambda z_1} \right) \\ &= \int dv_1 dv_2 t(v_1) t^*(v_2) \tilde{I}_s\left(\frac{u-v_1}{\lambda z_1} \right) \times \tilde{I}_s^*\left(\frac{u-v_2}{\lambda z_1} \right) D\left(\frac{v_2 - v_1}{\lambda z_0} \right), \end{aligned} \tag{11}$$

where $D(f)$ is the Fourier transform of $d(x)$. Equation (11) is very similar to the imaging formula of a partially coherent imaging system; thus we conclude that a LGI system with a bucket D_t can be regarded as a partially coherent imaging system. In particular, if the size of D_t is very large, we can take $d(x) = 1$ everywhere; then $D(f) = \delta(f)$, so Eq. (11) is reduced to

$$I(u) = \int dv |t(v)|^2 \left| \tilde{I}_s\left(\frac{u-v}{\lambda z_1}\right)\right|^2 = |t(v)|^2 \otimes \left| \tilde{I}_s\left(\frac{u-v}{\lambda z_1}\right)\right|^2. \tag{12}$$

This equation describes the image formation in an incoherent imaging system. As in the ordinary imaging theory [13], an OTF can be derived:

$$H_o(f) = \int df' I_s(-\lambda z_1(f+f'))I_s^*(-\lambda z_1 f'). \tag{13}$$

From these results, we see that when D_t changes from a pointlike detector to a very large bucket detector, the LGI system behavior changes from that of a coherent imaging system to that of a partially coherent imaging system, and finally to that of a fully incoherent imaging system. Also, since it is very easy to shape the distribution of the source intensity $I_s(x)$, both the ATF and OTF can be engineered according to experimental requirements. Thus, a LGI system provides a convenient method to optimally image an object.

For the Gaussian source considered in Sec. II, the OTF is

$$H_o(\vec{f}) = \exp\left(-\frac{\lambda^2 z_1^2 f^2}{2a_0^2}\right).$$

Now the cutoff frequency is $f_o = 3a_0/(\lambda z_1)$, a little larger than in the case with a pointlike D_t.

IV. DEFOCUSING EFFECTS

When the imaging condition is not exactly satisfied, i.e., $z_1 \neq z_2$, there are defocusing effects in the image formation. Suppose $z_2 - z_1$ is small, then another length l, defined as

$$\frac{1}{l} = \frac{1}{z_2} - \frac{1}{z_1}, \tag{14}$$

is very large. Thus Eq. (5) will be

$$h(u,v) = \int dx\, I_s(x) e^{(i\pi/\lambda l)x^2} e^{-(i2\pi/\lambda)(u/z_2 - v/z_1)x} = \tilde{P}\left(\frac{Mu-v}{\lambda z_1}\right), \tag{15}$$

where $\tilde{P}(f)$ is the Fourier transform of the defocused pupil function $P(x) = I_s(x)e^{(i\pi/\lambda l)x^2}$, and $M = z_1/z_2$ is the amplified factor.

With the help of Eq. (15), the imaging formula of a defocused LGI system with a bucket D_t will be

$$I(u) = \int dv_1 dv_2 t(v_1) t^*(v_2) \tilde{P}\left(\frac{Mu - v_1}{\lambda z_1}\right) \times \tilde{P}^*\left(\frac{Mu - v_2}{\lambda z_1}\right) D\left(\frac{v_2 - v_1}{\lambda z_0}\right). \tag{16}$$

Compared with Eq. (11), we see that the effect of defocusing is obtained by using $\tilde{P}$ to instead $\tilde{I}_s$.

Now, for a pointlike D_t, $d(x) = \delta(x)$, so $D(f) = 1$, and the defocused ATF is

$$H_c(f) = P(-\lambda z_1 f). \tag{17}$$

On the other hand, for a very large bucket D_t, $d(x) = 1$, so $D(f) = \delta(f)$, and the defocused OTF has the form

$$H_o(f) = \int df' P(-\lambda z_1(f+f'))P^*(-\lambda z_1 f'). \tag{18}$$

For the previously studied Gaussian source, the defocused pupil function is

$$P(x) = \exp\left[-\left(\frac{1}{a_0^2} - \frac{i\pi}{\lambda l}\right)x^2\right],$$

leading to

$$H_c(f) = \exp\left[-\left(\frac{1}{a_0^2} - \frac{i\pi}{\lambda l}\right)(\lambda z_1 f)^2\right],$$

$$H_o(f) = \exp\left[-\left(\frac{1}{2a_0^2} + \frac{\pi^2 a_0^2}{2\lambda^2 l^2}\right)(\lambda z_1 f)^2\right].$$

For the ATF, compared with Sec. II, f_c and the bandwidth will not be changed. The effect of defocusing is the introduction of phase distortions within the passband. The phase distortions still may have a severe effect on the quality of the LGI system.

On the other hand, for a LGI system with a large bucket D_t, the defocusing effects are very significant. Both the amplitude and phase of the OTF may be greatly changed. The cutoff frequency will be decreased,

$$f_o = \frac{3a_0}{\lambda z_1}\left(1 + \frac{\pi^2 a_0^4}{\lambda^2 l^2}\right)^{-1/2}.$$

Compared with the result in Sec. III, in addition to the phase distortions, the passband is also narrowed; thus the image will be greatly blurred. When the imaging condition severely deviates, l will be small, leading to a very small f_o, and the LGI system may not produce an image of the object.

Currently, there are two defocused LGI experiments [11,12]. In Ref. [12], $a_0 = 1.58$ mm, $\lambda = 632$ nm, and $z_1 = 484$ mm. Since a large bucket detector is used, we can use the OTF to analyze the experiment. When the imaging condition is satisfied, $f_o = 15.47$ mm^{-1}. In the defocused case, $z_2 = 534$ mm, the cutoff frequency is reduced to $f_o = 5.96$ mm^{-1}. Since the object is a double slit with width of 300 μm, the minimum spatial frequency of the object is around 3.33 mm^{-1}. This value is less than both the in-focus and defocused f_o, so the test object can be well imaged, just as reported in Ref. [12]. Also, our theory can be used to analyze the experiment in Ref. [11] if the needed parameter a_0 is known.

V. NUMERICAL SIMULATIONS

Now, we use numerical simulations to give some quantitative discussions on our theoretical results. For the LGI system, we choose $a_0 = 1.58$ mm, $\lambda = 632$ nm, $z_1 = 484$ mm, and $z_0 = 200$ mm. In all figures, the intensities are normalized to the maximum values.

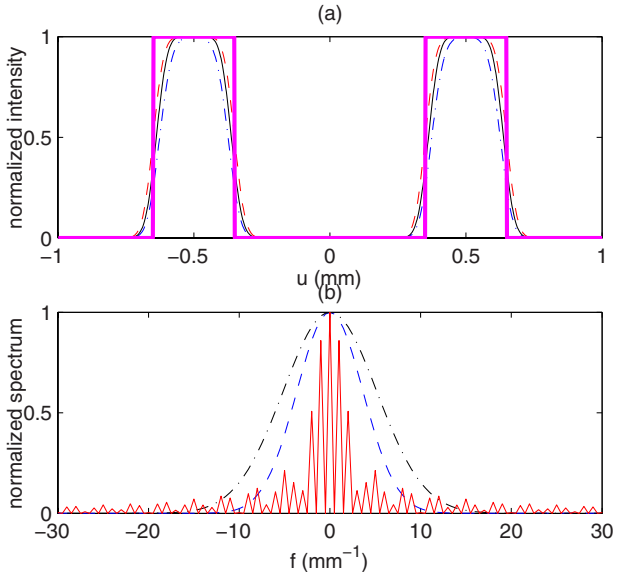

FIG. 2. (Color online) (a) Simulated images for a double-slit object. The thick solid line is the original object. The dash-dotted blue line is the image obtained with a pointlike detector. The thin solid black line is the image obtained with a finite size (1.5 mm) detector. The dashed red line is the image with a very large bucket detector. (b) The solid red line is the spectrum of the object. The dashed blue line is $H_c(f)$ when a pointlike D_t is used. The dash-dotted black line is $H_o(f)$ when a bucket D_t is used.

In the first example, the object is a double slit, with slit width 0.3 mm and slit distance 1.0 mm. When the imaging condition is satisfied, $z_2=z_1$, in Fig. 2, we plot the simulated images with three different kinds of detector D_t. The differences of these curves are small, but it is still very clear to see how the LGI system is transformed from a coherent imaging system to a partially coherent imaging system, and finally to a fully incoherent imaging system, when the size of D_t is increased. Because the OTF is wider than the ATF [Fig. 2(b)], using a bucket D_t improves the imaging quality.

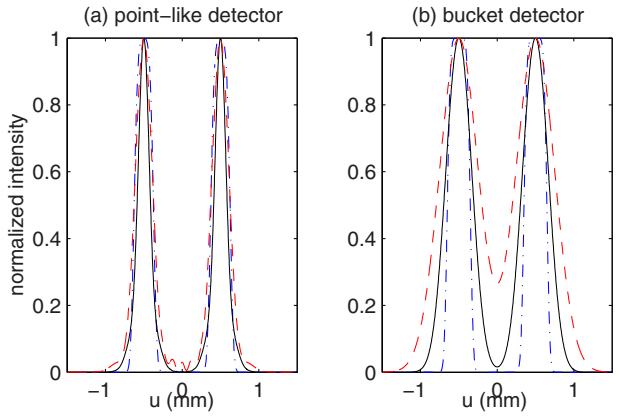

FIG. 3. (Color online) Defocus effects in a LGI system for a double-slit object. (a) A pointlike D_t is used to realize coherent imaging function. Dash-dotted blue line: $z_2=z_1$, no defocus. Solid black line: $z_2=584$ mm. Dashed red line: $z_2=684$ mm. (b) The same as (a), but a bucket D_t is used to realize the incoherent imaging function.

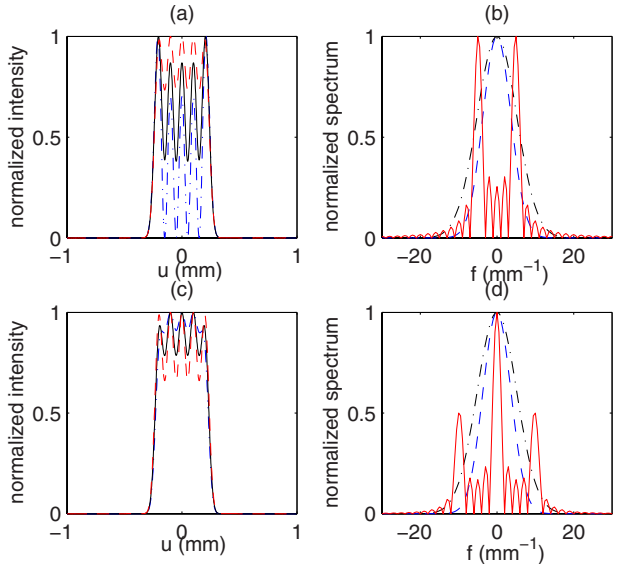

FIG. 4. (Color online) Simulated images for two sinusoidally modulated objects; one is $t_1(v)=\cos(\pi v/0.1)$ (a), (b), and the other is $t_2(v)=\cos^2(\pi v/0.1)$ (c),(d). (a),(c) The dash-dotted blue line is the image with a pointlike detector; the solid black line is the image with a finite size (1.0 mm) detector; the dashed red line is the image with a very large bucket detector. (b),(d) The solid red line is the spectrum of the object; the dashed blue line is $H_c(f)$ when a pointlike D_t is used; the dash-dotted black line is $H_o(f)$ when a bucket D_t is used.

The defocusing effects are clearly seen in Fig. 3, in which simulated images with three different z_2 are compared. When z_2 changes from 484 to 584 and to 684 mm, the images are degraded. The deviations are more significant for a bucket D_t compared with a pointlike D_t. When there is defocusing, the

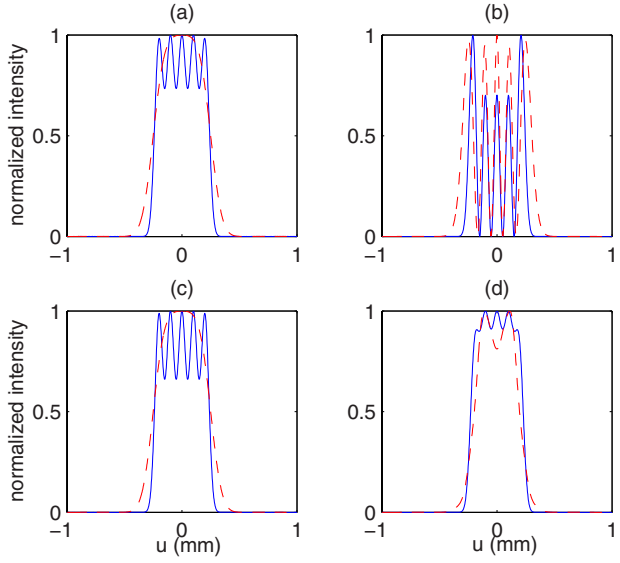

FIG. 5. (Color online) Defocusing effects in a LGI system for two sinusoidally modulated objects. Bucket D_t's are used in (a) and (c) to realize the incoherent imaging function. Pointlike D_t's are used in (b) and (d) to realize the coherent imaging function. (a) and (b) are images of the object t_1, (c) and (d) are images of t_2. Solid blue lines, $z_2=z_1$, no defocusing; dashed red line, $z_2=534$ mm.

images with a pointlike D_t are a little better than the images with a bucket D_t, as was discussed in the end of last section.

To see the effects of the detector and defocusing more clearly, two other objects are used in numerical simulation. The transmittance of the objects is considered to be sinusoidally modulated, $t_1(v)=\cos(\pi v/0.1)$, $t_2(v)=\cos^2(\pi v/0.1)$, and the size of these two objects is 0.5 mm. $t_1(v)<0$ means there is a π phase change at position v, so $t_1(v)$ represents an object with phase sensitivity, while $t_2(v)$ is phase insensitive. Because phase information about the object will be lost in the incoherent imaging, we find a pointlike D_t is superior to imaging t_1, while a bucket D_t is good to image t_2, as shown in Fig. 4. The transition from coherent to incoherent imaging is clearly demonstrated in these figures.

The defocusing effects with these two objects are given in Fig. 5. For bucket D_t, from Figs. 5(a) and 5(c), we find that the oscillating structures are totally smoothed when $z_2=534$ mm. For pointlike D_t [Figs. 5(b) and 5(d)], the images are broaden, and some structures are distorted. We can see that a pointlike D_t can image an object with phase changes very well even under defocusing conditions.

VI. CONCLUSION

In conclusion, we have studied the transfer functions in lensless ghost-imaging systems. We found that the LGI system can be transformed from a coherent imaging system to a partially coherent imaging system, and finally to a fully incoherent imaging system by changing the test detector from a pointlike detector to a finite bucket detector, and finally to a very large bucket detector. We obtain the amplitude transfer function or optical transfer function in LGI systems with a pointlike or bucket detector. When the imaging conditions are not exactly satisfied, we derived the defocused ATF and defocusing OTF, which can be used to investigate the defocusing effects. With the help of these transfer functions, we can quantitatively study the imaging ability of lensless ghost-imaging systems. Our results are demonstrated for a Gaussian-type source. Increasing the size of the source will increase the cutoff frequency of the LGI system, and enhance the imaging quality. From numerical simulations, we find that a pointlike D_t is superior for imaging an object with phase information, while a bucket D_t is good to image an object with only amplitude changes.

ACKNOWLEDGMENTS

J.C. is supported by the National Natural Science Foundation of China (Grants No. 10404031, and No. 10774047) and the SCUT BaiRen Program.

[1] A. Gatti, M. Bache, D. Magatti, E. Brambilla, F. Ferri, and L. A. Lugiato, J. Mod. Opt. **53**, 739 (2006), and references therein.
[2] D. V. Strekalov, A. V. Sergienko, D. N. Klyshko, and Y. H. Shih, Phys. Rev. Lett. **74**, 3600 (1995).
[3] T. B. Pittman, Y. H. Shih, D. V. Strekalov, and A. V. Sergienko, Phys. Rev. A **52**, R3429 (1995).
[4] J. Cheng and S. Han, Phys. Rev. Lett. **92**, 093903 (2004).
[5] A. Gatti, E. Brambilla, M. Bache, and L. A. Lugiato, Phys. Rev. Lett. **93**, 093602 (2004).
[6] F. Ferri, D. Magatti, A. Gatti, M. Bache, E. Brambilla, and L. A. Lugiato, Phys. Rev. Lett. **94**, 183602 (2005).
[7] D. Z. Cao, J. Xiong, and K. G. Wang, Phys. Rev. A **71**, 013801 (2005).
[8] D. Zhang, Y. H. Zhai, L. A. Wu, and X. H. Chen, Opt. Lett. **30**, 2354 (2005).
[9] J. Cheng and S. Han, Phys. Rev. A **76**, 023824 (2007).
[10] M. H. Zhang, Q. Wei, X. Shen, Y. F. Liu, H. L. Liu, J. Cheng, and S. S. Han, Phys. Rev. A **75**, 021803(R) (2007).
[11] G. Scarcelli, V. Berardi, and Y. Shih, Appl. Phys. Lett. **88**, 061106 (2006).
[12] L. Basano and P. Ottonello, Appl. Phys. Lett. **89**, 091109 (2006).
[13] J. W. Goodman, *Introduction to Fourier Optics* (Roberts and Company, Greenwood Village, 2005).
[14] M. Born and E. Wolf, *Principles of Optics* (Cambridge University, Cambridge U.K., 1999).